All-Optical Ultrafast Valley Switching in Two-Dimensional Materials

Navdeep Rana◉ and Gopal Dixit*

Department of Physics, Indian Institute of Technology Bombay, Powai, Mumbai 400076, India

Electrons in two-dimensional materials possess an additional quantum attribute, the valley pseudospin, labeled as **K** and **K′**—analogous to the spin up and spin down. The majority of research to achieve valley-selective excitations in valleytronics depends on resonant circularly polarized light with a given helicity. Not only acquiring valley-selective electron excitation but also switching the excitation from one valley to another is quintessential for bringing valleytronics-based technologies in reality. Present work introduces a coherent control protocol to initiate valley-selective excitation, de-excitation, and switch the excitation from one valley to another on the fly within tens of femtoseconds — a timescale faster than any valley decoherence time. Our protocol is equally applicable to *both* gapped and gapless two-dimensional materials. Monolayer graphene and molybdenum disulfide are used to test the universality. Moreover, the protocol is robust as it is insensitive to significant parameters of the protocol, such as dephasing times, wavelengths, and time delays of the laser pulses. Present work goes beyond the existing paradigm of valleytronics, and opens an alternative realm of valley switch at petahertz rate.

I. INTRODUCTION

The successful synthesis of monolayer graphene has led to the proliferation in synthesizing of other two-dimensional (2D) materials, such as hexagonal boron nitride and transition-metal dichalcogenides [1–3]. These 2D materials exhibit attractive transport and optoelectronic properties, which hold promise for upcoming technologies [4]. One of the fascinating features of these 2D materials is the electron's additional quantum attribute, the valley pseudospin — analogous to the electron's spin. The valley pseudospin is associated with the valleys in the energy landscape of these materials. The hexagonal 2D materials are endowed with two degenerate valleys situated at the corners of the Brillouin zone [5,6]. The flexible control over these valley pseudospins offers a platform to write, process, and store quantum information [7,8]. Moreover, coherent switching of electron excitation from one valley to another, on a timescale faster than the valley decoherence, is quintessential for valleytronics-based emerging quantum technologies at ambient conditions [9,10].

Owing to the sign of the Berry curvature and resultant selection rules, left- or right-handed circularly polarized light, resonant to the material's band gap, has been employed to achieve valley-selectivity excitation in gapped 2D materials [11–17]. In recent years, nonresonant laser pulses with tailored waveforms have been applied to obtain desired valley excitation in gapped 2D materials [18–21]. Similar significant success has been reported in gapless 2D materials [22–28]. Huber and co-workers have experimentally achieved a milestone in coherent valley switching by using a combination of a pump pulse, resonant with the band gap in tungsten diselenide, and a controlled terahertz pulse [29]. Recently, a scheme consisting of a pair of two time-separated orthogonally polarized linear pulses has been proposed for valley excitation in gapped 2D materials [30]. Moreover, it has been shown that the desired control over valley excitation can be obtained by controlling the delay between the two pulses and their polarizations [30]. Ivanov and co-workers have proposed a control protocol to initiate and switch the valley excitation in gapped 2D materials using a sequence of four time-separated orthogonally polarized linear pulses [31]. Linear pulses, resonant with the band gap of the 2D materials, are used in both schemes [30,31]. Thus, they are unsuitable for gapless 2D materials, such as graphene. Moreover, both the schemes are susceptible to the relative polarizations and delay among the linear pulses. Thus, a robust and universal control protocol, applicable to gapped and gapless 2D materials, is lacking—a major impediment in the realization of versatile light-based valleytronics devices.

In this work, we provide a universal control protocol for initiating and switching the excitation from one valley to another on timescales faster than valley decoherence time. To demonstrate universality, we apply our protocol to gapped and gapless 2D materials. Monolayer molybdenum

disulfide (MoS$_2$) and graphene will be used to represent gapped and gapless 2D materials, respectively.

The direction of electron flow is sensitive to the exact shape of the electric field waveform of the laser, which can be steered by the carrier-envelope phase (CEP) with attosecond precision. Recently, precise sculpting the waveforms of one and few-cycle laser pulses via multioctave shaping has been demonstrated experimentally [32–35]. Linearly polarized laser pulses with CEP = 0° and = 180° have the electric field waveform opposite in direction. Thus, choosing few-cycle laser pulses with well-defined CEP is expected to facilitate switching the excitation from one direction to another, which is the essence of our protocol.

Let us understand how few-cycle CEP-stabilized linear pulse can induce valley polarization. It is known that the canonical momenta is conserved at each instant of time during laser-solid interaction, i.e., $\mathbf{k}(t_2) - \mathbf{A}(t_2) = \mathbf{k}(t_1) - \mathbf{A}(t_1)$ where t_1 and t_2 are two arbitrary instances during the laser pulse, $\mathbf{k}$ is the crystal momentum, and $\mathbf{A}(t)$ is the vector potential of the laser. The probability of an electron excitation from valence to conduction band is maximum at $\mathbf{K}$ and $\mathbf{K}'$ valleys, i.e., near minimum band gap. Moreover, the likelihood of the excitation is maximum when the electric field strength of the laser is maximum. Thus, the maximum number of electrons are excited into the conduction band near the maxima of the electric field. Note that there is no preference for electron ejection between the two valleys as both valleys are energetically equivalent.

As the laser pulse gets over, the electronic populations from the $\mathbf{K}$ and $\mathbf{K}'$ valleys are shifted to $\mathbf{k}_1$ and $\mathbf{k}_2$ as $\mathbf{K} = \mathbf{k}_1(t \rightarrow \infty) + \mathbf{A}(t_0)$ and $\mathbf{K}' = \mathbf{k}_2(t \rightarrow \infty) + \mathbf{A}(t_0)$ with t_0 as the time at which the electric field is maximum. The population distribution associated with the electron excitation is symmetric when the maxima of the electric field coincide with the zero of the vector potential, which is true for a longer laser pulse. Thus, "relatively" longer pulse yields symmetric electron excitation around $\mathbf{K}$ and $\mathbf{K}'$ valleys and, therefore, no valley polarization. This situation changes drastically as the pulse becomes shorter and sensitive to the CEP. In the case of the few-cycle CEP-sensitive pulse, the maxima of the electric field does not coincide with the zero of the vector potential. The value of the vector potential is sensitive to the value of the CEP. Thus, the nonzero value of the vector potential at t_0 creates asymmetric population distribution around $\mathbf{K}$ and $\mathbf{K}'$ valleys [36]. The direction of the electron excitation is dictated by the direction of the field amplitude. For CEP value of 0°, the magnitude of the vector potential is positive at the maximum of electric field, which favors $\mathbf{K}'$ valley over $\mathbf{K}$. On the other hand, as the CEP changes to 180°, the magnitude of the vector potential becomes negative and thus $\mathbf{K}$ valley is favored.

The key idea of our valley-switching protocol by an all-optical means in a 2D material, with two degenerate valleys at $\mathbf{K}$ and $\mathbf{K}'$, is illustrated in Fig. 1. Coherent switching of an electron excitation from one valley to another in a 2D material can be envisioned as a three-step process: in the first step, a linear laser pulse induces a preferable valley excitation at $\mathbf{K}'$ over $\mathbf{K}$. An application of a second linear pulse during the second step could counterbalance the preferred valley excitation at $\mathbf{K}'$ by reversing the direction of the excitation. The final step involves the action of a third linear pulse, similar to the one used in the second step, which would manage the excitation away from $\mathbf{K}'$ valley as it favors the excitation to $\mathbf{K}$ valley. Thus, switching of the valley excitation from one to another can be potentially realized by the action of three time-separated CEP-controlled linear pulses polarized along the same direction. Our approach is simpler than the one discussed in Ref. [31] where a sequence of four orthogonally polarized linear pulses, resonant with the band gap of a 2D material, is used. Furthermore, as we demonstrate below, our protocol is robust against several limitations in the experimental setup as it is insensitive to the wavelengths of the laser pulses, time delay among the pulses, and dephasing time. The protocol discussed in Ref. [31] is susceptible to the experimental setup.

II. COMPUTATIONAL DETAILS

The nearest-neighbour tight-binding approximation is used to obtain the electronic ground state of gapped and gapless graphene. The corresponding Hamiltonian is expressed as

$$\mathcal{H}_{\mathbf{k}} = -\gamma_0 f^*(k)\hat{a}_{\mathbf{k}}^{\dagger}\hat{b}_{\mathbf{k}} - \frac{\Delta}{2}\hat{a}_{\mathbf{k}}^{\dagger}\hat{a}_{\mathbf{k}} + \frac{\Delta}{2}\hat{b}_{\mathbf{k}}^{\dagger}\hat{b}_{\mathbf{k}} + \text{H.c.} \quad (1)$$

Here, γ_0 is the nearest-neighbor hopping energy, $\hat{a}_k^{\dagger}(\hat{b}_k)$ is creation (annihilation) operator corresponding to the $A(B)$ type of the atom in the unit cell. $f(k)$ is defined as $\sum_{i \in nn} e^{i\mathbf{k}\cdot\mathbf{d}_i}$ with $\mathbf{d}_i$ as the separation vector between an atom with its nearest neighbor [37–39]. The band structure of the 2D material is obtained by solving Eq. (1). To obtain the minimum band gap at $\mathbf{K}$ and $\mathbf{K}'$ points, we use $\Delta = 0$ and 1.58 eV for graphene and MoS$_2$, respectively.

Semiconductor-Bloch equations in Houston basis are used to simulate the electron dynamics in the presence of few-cycle laser pulses [40] and defined as

$$\frac{d}{dt}\rho_{vv}^{\mathbf{k}} = i\mathbf{E}(t) \cdot \mathbf{d}_{vc}(\mathbf{k}_t)\rho_{cv}^{\mathbf{k}} + \text{c.c.} \quad (2a)$$

$$\frac{d}{dt}\rho_{cv}^{\mathbf{k}} = -\left[i\varepsilon_{cv}(\mathbf{k}_t) + \frac{1}{T_2}\right]\rho_{cv}^{\mathbf{k}}$$
$$+ i\mathbf{E}(t) \cdot \mathbf{d}_{cv}(\mathbf{k}_t)\left[\rho_{vv}^{\mathbf{k}} - \rho_{cc}^{\mathbf{k}}\right]. \quad (2b)$$

Here, $\mathbf{k}_t$ stands for $\mathbf{k} + \mathbf{A}(t)$, $\mathbf{E}(t)$ is the electric field of the laser and T_2 represents a phenomenological dephasing
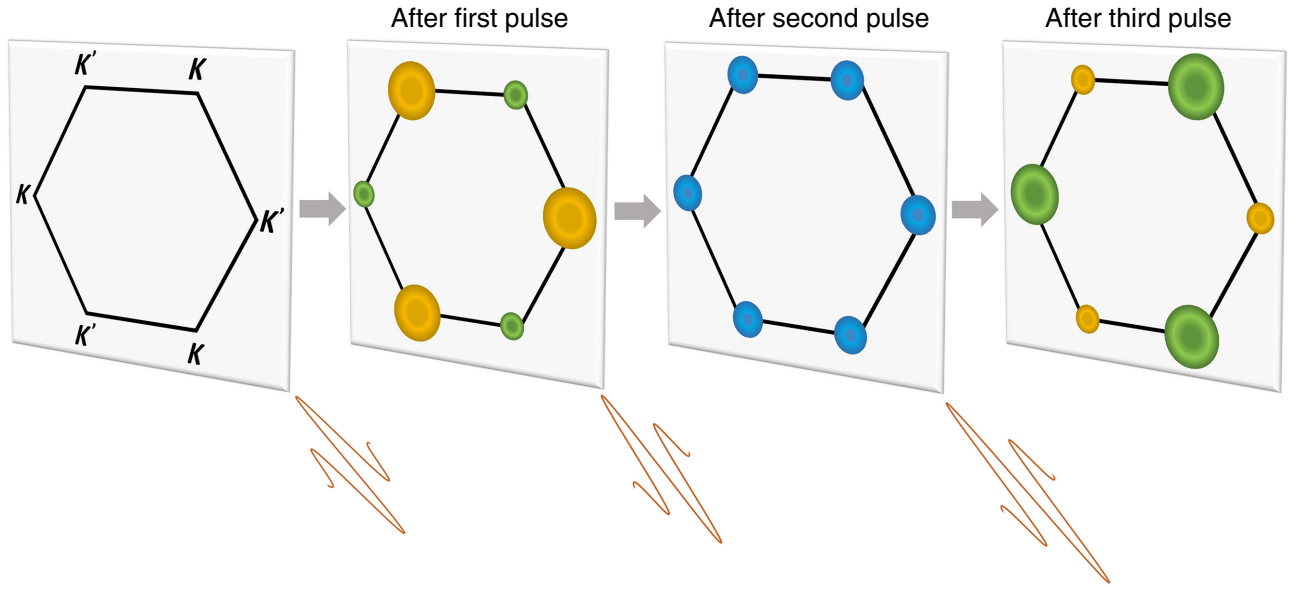
FIG. 1. Schematic of an all-optical ultrafast valley switch in a two-dimensional material. First panel: Brillouin zone of a 2D material along with high-symmetry points in momentum space. Two degenerate valleys are located at the corners of the Brillouin zone, i.e., at **K** and **K**′. Second panel: valley excitation at **K**′ (shown in yellow) is favored over **K** (shown in green) after the end of the first linear pulse. Third panel: the favored valley excitation at **K**′ is counterbalanced by the second linear pulse subsequently as shown in blue. Fourth panel: reversal in the preference of valley excitation at **K** (shown in green) over **K**′ (shown in yellow) by the action of the third linear pulse. All three few-cycle pulses have well-defined carrier-envelope phase and are linearly polarized along $\Gamma - \mathbf{K}$ direction.

term to incorporate the decoherence between electrons and holes. $\mathbf{d}_{cv}(\mathbf{k}) = i\langle c, \mathbf{k}|\nabla_{\mathbf{k}}|v, \mathbf{k}\rangle$, and $\varepsilon_{cv}(\mathbf{k})$ are the dipole matrix element and band-gap energy between conduction and valence bands at **k**, respectively. Note that $\rho_{cc}^{\mathbf{k}}(t) = 1 - \rho_{vv}^{\mathbf{k}}(t)$, and $\rho_{vc}^{\mathbf{k}}(t) = \rho_{cv}^{\mathbf{k*}}(t)$. The electronic population of the conduction band is estimated using $n^{\mathbf{k}}(t) = \rho_{cc}^{\mathbf{k}}(t)$.

To demonstrate the robustness of our idea, the parameters of the three laser pulses are similar for graphene and MoS_2. Realistic two-cycle pulses with well-defined CEP are used in our control protocol. All three pulses have a wavelength of 2.0 μm with cosine squared envelope, and are linearly polarised along k_x direction, i.e., the zigzag ($\Gamma - \mathbf{K}$) direction. The CEP of the first, second, and third pulses are 0°, 180°, and 180°, respectively. For graphene, the peak intensities of the first, second, and third pulses are 3.8×10^{12}, 3.8×10^{12}, and 4.4×10^{12} W/cm², respectively. The peak intensities of the three pulses are slightly tuned to optimize valley switching in MoS_2. In this case, the peak intensities of the first, second, and third pulses are 2.6×10^{12}, 2.6×10^{12}, and 3.0×10^{12} W/cm², respectively. In both cases, the intensity of the third pulse is slightly higher than the second one to favor the electron excitation to another valley. However, the ratios of the three pulses are kept constant in graphene and MoS_2. Note that the intensities of the laser pulses are close to the damage threshold of monolayer graphene [41]. By using an appropriate substrate, damage of the sample can be further avoided.

III. RESULTS AND DISCUSSION

Let us first discuss monolayer graphene's numerical results to confirm our valley switching protocol. There are two equivalent valleys at **K** and **K**′ as evident from the energy band structure of graphene along high-symmetry points in the first Brillouin zone, see Fig. 2(a). The band dispersion is linear, and energy gaps between valence and conduction bands at **K** and **K**′ valleys are zero. Thus, schemes based on resonant laser pulses for valley-selective excitation are not suited for graphene.

The residual electronic populations in the conduction band after the first, second, and third pulses are presented in Figs. 2(b)–2(d), respectively. The populations in the vicinity of **K** and **K**′ are shown by red and blue, respectively. After the first pulse, the residual population is asymmetric. Moreover, the population in **K**′ valley is more in comparison to the **K** valley as reflected from Fig. 2(b).

Let us uncover the underlying mechanism for the preferential population in **K**′ valley by the first laser pulse. As discussed earlier, the exact shape of the waveform of an intense laser dictates the direction of the electron's motion, either positive or negative, along the x axis. Also, a sufficiently intense laser not only excites electrons in the valley but also its vicinity. As the time starts, electrons are driven towards a positive direction as the vector potential of the first laser has a negative slope and increases in the same direction. At some point in time, electrons change their direction of motion from positive to negative due to a
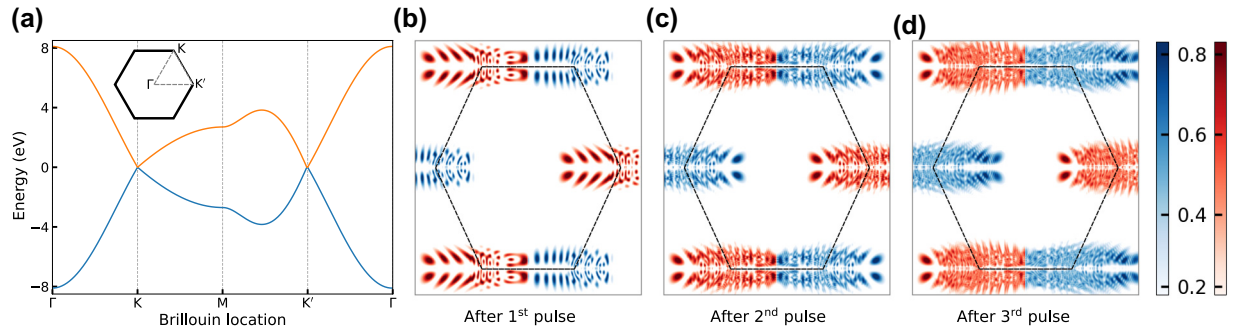
FIG. 2. All-optical valley switch in graphene. (a) Energy band structure of graphene along high-symmetry points in the Brillouin zone. Two inequivalent and degenerate valleys located at the corners of the Brillouin zone with crystal momenta **K** and **K**′. The first Brillouin zone is shown in the inset. The momentum-resolved residual electronic populations in the first Brillouin zone of the conduction band are shown in (b)–(d) after the end of the first, second, and third linear pulses, respectively. (b) The first pulse with CEP = 0° results in asymmetric electronic population, leading to preferred excitation around **K**′ valley. (c) After the second pulse with CEP = 180°, symmetric residual population in the Brillouin zone, i.e., **K** and **K**′ valleys have equal population. (d) Asymmetric population distribution with more in the vicinity of **K** valley. Thus, switch of excitation from **K**′ to **K** valley after the end of the third pulse with CEP = 180°. Red and blue represent the residual populations around **K**′ and **K** valleys, respectively.

change in the slope of the vector potential from negative to positive as the potential peaks twice during each half cycle of the waveform. The two paths of the electron motion lead an interference, which results in interference fringes in the residual population as evident from Fig. 2(b) [see Video S1 within the Supplemental Material [42]]. Due to zero CEP of the pulse, the vector potential is asymmetric and has a net positive component, which leads the **K**′ valley to be more populated over **K** valley. Thus, the asymmetry of the laser waveform gets imprinted in the asymmetric residual populations.

The preference for excitation from one valley to another can be altered by changing the CEP from 0° to 180°. To counterbalance the preferred population in **K**′ valley caused by the first pulse, let us employ a second pulse with

CEP = 180° that favors the population in **K** valley. Thus, the combined effect of both pulses leads to a symmetric residual population around both valleys as reflected from Fig. 2(c).

To break the equal population distribution around **K** and **K**′, a third pulse with CEP = 180° is applied, which induces asymmetric residual population. However, this time **K** valley has a more residual population over the **K**′ valley, see Fig. 2(d). Thus, the action of three time-separated linear pulses switches the population from one valley to another completely [42]. Moreover, the switch of valley excitation from **K**′ to **K** valley occurs within a few tens of femtoseconds — an order of magnitude faster than the valley decoherence time [9,10]. Note that two-cycle laser pulses with CEP = 90° and 270° have zero
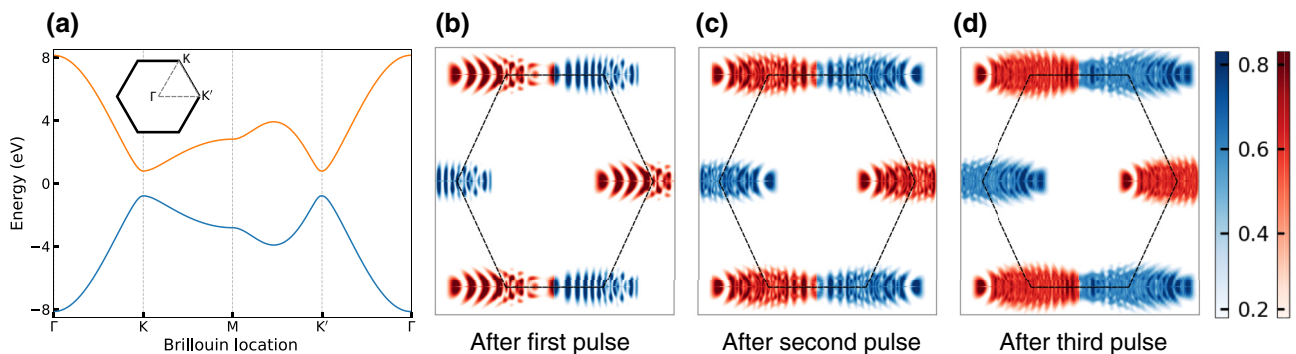

FIG. 3. All-optical valley switch in MoS$_2$. (a) Energy band structure of MoS$_2$ displays two valleys along high-symmetry points at **K** and **K**′. Energy band gaps at **K** and **K**′ are 1.58 eV. The momentum-resolved residual electronic populations in the first Brillouin zone of the conduction band after the end of the first, second, and third laser pulses are shown in (b)–(d), respectively. Red and blue represent the residual populations around **K**′ and **K** valleys, respectively. The details of the linear pulses and the residual populations in (b)–(d) are the same as in Fig. 2.
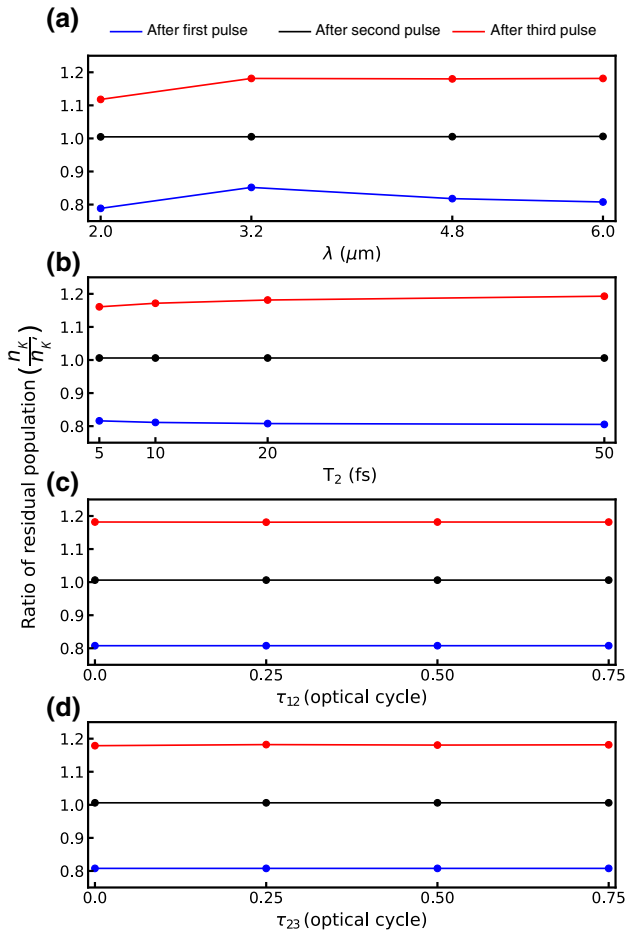
FIG. 4. Robustness of our protocol with respect to laser parameters and dephasing time. The ratio of residual population in the conduction band around K and K' valleys ($n_K/n_{K'}$) with respect to (a) laser's wavelength λ, (b) dephasing time T_2, time delay between (c) the first and second laser pulses τ_{12}, and (d) the second and third laser pulses τ_{23}. Time delay between the second and third laser is constant in (c), and the delay between the first and second laser is constant in (d). The wavelength of all three pulses is kept the same in (a). The residual populations after the first, second, and third pulses are shown by blue, black, and red, respectively.

net components and do not prefer any valley-selective excitation.

After a successful illustration of valley switching in gapless graphene, let us explore the universality of our control protocol. For this purpose, we apply our protocol to MoS$_2$, which belongs to another class of 2D materials, i.e., gapped graphene. As evident from Fig. 3(a), there are two valleys at K and K' with a band gap of 1.58 eV, which makes MoS$_2$ a semiconductor in nature. To claim the universality, the sequence of the three time-separated laser pulses are the same for MoS$_2$ as for graphene.

The residual population in the conduction band after the end of the first pulse is shown in Fig. 3(b). As evident from the figure, the first pulse with CEP $= 0°$ favors electron excitation in K' valley. The second pulse with CEP $= 180°$ dispenses the population equally to both K and K' valleys [see Fig. 3(c)]. The valley excitation is completely switched to K valley by the action of the third pulse with CEP $= 180°$ as reflected from Fig. 3(d). The results presented in Fig. 3 unequivocally establish that our protocol with the same setup, as in graphene, is equally applicable to MoS$_2$ for a complete switch of valley excitation from one valley to another. Thus, our control protocol of valley switch is equally applicable to gapped and gapless 2D materials, unlike the protocol discussed in Ref. [31].

After establishing valley switching in graphene and MoS$_2$, let us explore the robustness of our protocol concerning the various parameters in an experimental setup. To this end, we analyze the ratio of the residual population in graphene after the end of the first, second, and third laser pulses, as shown by blue, black, and red lines [See Fig. 4]. As illustrated earlier, the residual population in the K' valley is greater than the K valley, so the ratio is less than one. However, the ratio becomes one after the end of the second pulse as it counterbalances the population in both the valleys. The action of the third pulse favors the residual population in the K valley, and hence the ratio becomes more than one. It is expected that the change in the wavelength of the laser pulses does not affect the outcome of the valley switch from K' to K as the underlying mechanism relies on tuning the CEP of the pulses. The results in Fig. 4(a) confirm our expectations as our protocol of the valley switch is insensitive with respect to the change in the wavelength from 2.0 to 6.0 μm for all the three pulses. Intensity ratios of the three pulses are kept constant while varying the wavelengths.

It has been anticipated that the coherence between electron and hole at their respective energy bands is a crucial factor in the functioning of light-driven valleytronics devices [9]. Thus, it is essential to check how our protocol depends on the electron-hole coherence. The residual populations after the end of the three pulses are presented for different dephasing time T_2, which determines the decoherence between electron and hole. As evident from Fig. 4(b), the ratios of the populations remain unaffected for different values of T_2, ranging from 5 to 50 fs. Invariance of the ratios with T_2 also indicates that the electron excitation by CEP-controlled laser pulses is dominated by the intraband motion [43].

It is natural to envisage that our control protocol is robust against the time delay among the three pulses as the populations ratio do not change with T_2. To verify this hypothesis, we present the population ratios for the different delays between the first and second pulses (τ_{12}) while keeping the delay between the second and third pulses constant [see Fig. 4(c)]. As evident from the figure,

the residual populations after the end of the three pulses remain the same for different values of τ_{12}. The same is true when the delay between the second and third pulses (τ_{23}) is changed, while τ_{12} is kept constant [see Fig. 4(d)]. Thus, the analysis of Figs. 4(c) and 4(d) demonstrate the protocol of valley switching is independent of the time delay among the three pulses, i.e., changes in τ_{12} and τ_{23}. The other parameters are kept identical as in Fig. 2, while varying τ_{12} and τ_{23}.

IV. CONCLUSION

In summary, we illustrate a coherent control protocol to switch the valley excitation from one valley to another in 2D materials on a timescale faster than any valley decoherence time. Our protocol consists of three time-separated two-cycle linear pulses, polarized along the same direction. For efficient valley switching, the electric field waveform of the employed pulses are tailored by tuning the CEP. We successfully illustrate the valley switch in graphene and MoS_2. Thus, our protocol is versatile as it relies on CEP-controlled nonresonant pulses and equally applicable to hexagonal gapped and gapless 2D materials. Moreover, our protocol is resilient to significant parameters in an experimental setup as it is oblivious to the wavelength of the pulses, time delay among pulses, and the dephasing time. The laser pulses used in our protocol have been recently employed to explore electron dynamics in solids [33,34,44]. Therefore, our protocol of valley switching is within reach of experimental feasibility. Additionally, the present work can be extended to realize logical operations using valley pseudospins — similar to the recent experimental work in graphene using real and virtual charge carriers [45]. We also test our protocol with CEP-controlled single-cycle pulses, and our findings remain qualitatively the same. However, valley polarization reduces drastically as the number of cycles in a laser pulse increases [36]. To end, high-harmonic spectroscopy and time-resolved angle-resolved photoemission spectroscopy could be employed to read the outcomes of the valley switching [46–49].

ACKNOWLEDGMENTS

[1] K. S. Novoselov, D. Jiang, F. Schedin, T. J. Booth, V. V. Khotkevich, S. V. Morozov, and A. K. Geim, Two-dimensional atomic crystals, Proc. Natl. Acad. Sci. **102,** 10451 (2005).

[2] Sajedeh Manzeli, Dmitry Ovchinnikov, Diego Pasquier, Oleg V. Yazyev, and Andras Kis, 2d transition metal dichalcogenides, Nat. Rev. Mater. **2,** 1 (2017).

[3] Kin Fai Mak, Changgu Lee, James Hone, Jie Shan, and Tony F. Heinz, Atomically Thin MoS_2: A New Direct-Gap Semiconductor, Phys. Rev. Lett. **105,** 136805 (2010).

[4] Kin Fai Mak and Jie Shan, Photonics and optoelectronics of 2d semiconductor transition metal dichalcogenides, Nat. Photonics **10,** 216 (2016).

[5] Xiaodong Xu, Wang Yao, Di Xiao, and Tony F. Heinz, Spin and pseudospins in layered transition metal dichalcogenides, Nat. Phys. **10,** 343 (2014).

[6] Fabio Bussolotti, Hiroyo Kawai, Zi En Ooi, Vijila Chellappan, Dickson Thian, Ai Lin Christina Pang, and Kuan Eng Johnson Goh, Roadmap on finding chiral valleys: Screening 2D materials for valleytronics, Nano Futures **2,** 032001 (2018).

[7] Kin Fai Mak, Di Xiao, and Jie Shan, Light–valley interactions in 2D semiconductors, Nat. Photonics **12,** 451 (2018).

[8] Ziliang Ye, Dezheng Sun, and Tony F. Heinz, Optical manipulation of valley pseudospin, Nat. Phys. **13,** 26 (2017).

[9] S. A. Vitale, D. Nezich, J. O. Varghese, P. Kim, N. Gedik, P. Jarillo-Herrero, D. Xiao, and M. Rothschild, Valleytronics: Opportunities, challenges, and paths forward, Small **14,** 1801483 (2018).

[10] J. R. Schaibley, H. Yu, G. Clark, P. Rivera, J. S. Ross, K. L. Seyler, W. Yao, and X. Xu, Valleytronics in 2D materials, Nat. Rev. Mater. **1,** 16055 (2016).

[11] K. F. Mak, K. He, J. Shan, and T. F. Heinz, Control of valley polarization in monolayer MoS_2 by optical helicity, Nat. Nanotechnol. **7,** 494 (2012).

[12] A. M. Jones, H. Yu, N. J. Ghimire, S. Wu, G. Aivazian, J. S. Ross, B. Zhao, J. Yan, D. G. Mandrus, and D. Xiao, et al., Optical generation of excitonic valley coherence in monolayer WSe_2, Nat. Nanotechnol. **8,** 634 (2013).

[13] D. Gunlycke and C. T. White, Graphene Valley Filter Using a Line Defect, Phys. Rev. Lett. **106,** 136806 (2011).

[14] D. Xiao, G. B. Liu, W. Feng, X. Xu, and W. Yao, Coupled Spin and Valley Physics in Monolayers of MoS_2 and Other Group-VI Dichalcogenides, Phys. Rev. Lett. **108,** 196802 (2012).

[15] Hualing Zeng, Junfeng Dai, Wang Yao, Di Xiao, and Xiaodong Cui, Valley polarization in MoS_2 monolayers by optical pumping, Nat. Nanotechnol. **7,** 490 (2012).

[16] Ting Cao, Gang Wang, Wenpeng Han, Huiqi Ye, Chuanrui Zhu, Junren Shi, Qian Niu, Pingheng Tan, Enge Wang, and Baoli Liu, et al., Valley-selective circular dichroism of monolayer molybdenum disulphide, Nat. Commun. **3,** 1 (2012).

[17] Kin Fai Mak, Kathryn L. McGill, Jiwoong Park, and Paul L. McEuen, The valley Hall effect in MoS_2 transistors, Science **344,** 1489 (2014).

[18] S. Azar Oliaei Motlagh, Fatemeh Nematollahi, Vadym Apalkov, and Mark I. Stockman, Topological resonance and single-optical-cycle valley polarization in gapped graphene, Phys. Rev. B **100,** 115431 (2019).

[19] S. Azar Oliaei Motlagh, Jhih-Sheng Wu, Vadym Apalkov, and Mark I. Stockman, Femtosecond valley polarization

and topological resonances in transition metal dichalcogenides, Phys. Rev. B **98**, 081406 (2018).

[20] Yong-Lin He, Jing Guo, Fang-Yan Gao, and Xue-Shen Liu, Dynamical symmetry and valley-selective circularly polarized high-harmonic generation in monolayer molybdenum disulfide, Phys. Rev. B **105**, 024305 (2022).

[21] Arqum Hashmi, Shunsuke Yamada, Atsushi Yamada, Kazuhiro Yabana, and Tomohito Otobe, Valley polarization control in WSe$_2$ monolayer by a single-cycle laser pulse, Phys. Rev. B **105**, 115403 (2022).

[22] R. V. Gorbachev, J. C. W. Song, G. L. Yu, AV Kretinin, F. Withers, Y. Cao, A. Mishchenko, I. V. Grigorieva, Konstantin S. Novoselov, and L. S. Levitov, *et al.*, Detecting topological currents in graphene superlattices, Science **346**, 448 (2014).

[23] M. Yankowitz, J. Xue, D. Cormode, J. D. Sanchez-Yamagishi, K. Watanabe, T. Taniguchi, P. Jarillo-Herrero, P. Jacquod, and B. J. LeRoy, Emergence of superlattice dirac points in graphene on hexagonal boron nitride, Nat. Phys. **8**, 382 (2012).

[24] M. M. Grujić, M. Ž. Tadić, and F. M. Peeters, Spin-Valley Filtering in Strained Graphene Structures with Artificially Induced Carrier Mass and Spin-Orbit Coupling, Phys. Rev. Lett. **113**, 046601 (2014).

[25] M. Settnes, S. R. Power, M. Brandbyge, and A. P. Jauho, Graphene Nanobubbles as Valley Filters and Beam Splitters, Phys. Rev. Lett. **117**, 276801 (2016).

[26] A. Rycerz, J. Tworzydło, and C. W. J. Beenakker, Valley filter and valley valve in graphene, Nat. Phys. **3**, 172 (2007).

[27] Arijit Kundu, H. A. Fertig, and Babak Seradjeh, Floquet-Engineered Valleytronics in Dirac Systems, Phys. Rev. Lett. **116**, 016802 (2016).

[28] Hamed Koochaki Kelardeh, Ulf Saalmann, and Jan M. Rost, Ultrashort laser-driven dynamics of massless Dirac electrons generating valley polarization in graphene, Phys. Rev. Res. **4**, L022014 (2022).

[29] F. Langer, C. P. Schmid, S. Schlauderer, M. Gmitra, J. Fabian, P. Nagler, C. Schüller, T. Korn, P. G. Hawkins, and J. T. Steiner, *et al.*, Lightwave valleytronics in a monolayer of tungsten diselenide, Nature **557**, 76 (2018).

[30] Sangeeta Sharma, Peter Elliott, and Sam Shallcross, Valley control by linearly polarized laser pulses: Example of WSe$_2$, Optica **9**, 947 (2022).

[31] Rui E. F. Silva, Misha Ivanov, and Álvaro Jiménez-Galán, All-optical valley switch and clock of electronic dephasing, Opt. Express **30**, 30347 (2022).

[32] Peter Krogen, Haim Suchowski, Houkun Liang, Noah Flemens, Kyung-Han Hong, Franz X. Kärtner, and Jeffrey Moses, Generation and multi-octave shaping of mid-infrared intense single-cycle pulses, Nat. Photonics **11**, 222 (2017).

[33] Y. Kawakami, T. Amano, H. Ohashi, H. Itoh, Y. Nakamura, H. Kishida, T. Sasaki, G. Kawaguchi, H. M. Yamamoto, and K. Yamamoto, *et al.*, Petahertz non-linear current in a centrosymmetric organic superconductor, Nat. Commun. **11**, 1 (2020).

[34] I. V. Savitsky, E. A. Stepanov, A. A. Lanin, A. B. Fedotov, and A. M. Zheltikov, Single-cycle, multigigawatt carrier–envelope-phase-tailored near-to-mid-infrared driver for strong-field nonlinear optics, ACS Photonics **9**, 1679 (2022).

[35] T. Higuchi, C. Heide, K. Ullmann, H. B. Weber, and P. Hommelhoff, Light-field-driven currents in graphene, Nature **550**, 224 (2017).

[36] M. S. Mrudul and Gopal Dixit, Controlling valley-polarisation in graphene via tailored light pulses, J. Phys. B **54**, 224001 (2021).

[37] M. S. Mrudul and Gopal Dixit, High-harmonic generation from monolayer and bilayer graphene, Phys. Rev. B **103**, 094308 (2021).

[38] M. S. Mrudul, High-harmonic spectroscopy of two-dimensional materials, Preprint ArXiv:2203.10253 (2022).

[39] Navdeep Rana, M. S. Mrudul, Daniil Kartashov, Misha Ivanov, and Gopal Dixit, High-harmonic spectroscopy of coherent lattice dynamics in graphene, Phys. Rev. B **106**, 064303 (2022).

[40] Navdeep Rana and Gopal Dixit, Probing phonon-driven symmetry alterations in graphene via high-order-harmonic spectroscopy, Phys. Rev. A **106**, 053116 (2022).

[41] Adam Roberts, Daniel Cormode, Collin Reynolds, Ty Newhouse-Illige, Brian J. LeRoy, and Arvinder S. Sandhu, Response of graphene to femtosecond high-intensity laser irradiation, Appl. Phys. Lett. **99**, 051912 (2011).

[42] See Supplemental Material at http://link.aps.org/supplemental/10.1103/PhysRevApplied.19.034056 for temporal evolution of valley excitation from one valley to another in monolayer graphene by the action of three CEP-stabilized two-cycle linearly polarized pulses. The description of the video can be found in the READMe.txt file.

[43] M. S. Mrudul, Álvaro Jiménez-Galán, Misha Ivanov, and Gopal Dixit, Light-induced valleytronics in pristine graphene, Optica **8**, 422 (2021).

[44] Dandan Hui, Husain Alqattan, Shunsuke Yamada, Vladimir Pervak, Kazuhiro Yabana, and Mohammed Th Hassan, Attosecond electron motion control in dielectric, Nat. Photonics **16**, 33 (2022).

[45] Tobias Boolakee, Christian Heide, Antonio Garzón-Ramírez, Heiko B. Weber, Ignacio Franco, and Peter Hommelhoff, Light-field control of real and virtual charge carriers, Nature **605**, 251 (2022).

[46] M. S. Mrudul, N. Tancogne-Dejean, A. Rubio, and G. Dixit, High-harmonic generation from spin-polarised defects in solids, npj Comput. Mater. **6**, 1 (2020).

[47] Amar Bharti, M. S. Mrudul, and Gopal Dixit, High-harmonic spectroscopy of light-driven nonlinear anisotropic anomalous hall effect in a Weyl semimetal, Phys. Rev. B **105**, 155140 (2022).

[48] S. Ghimire and D. A. Reis, High-harmonic generation from solids, Nat. Phys. **15**, 10 (2019).

[49] J. Reimann, S. Schlauderer, C. P. Schmid, F. Langer, S. Baierl, K. A. Kokh, O. E. Tereshchenko, A. Kimura, C. Lange, and J. Güdde, *et al.*, Subcycle observation of lightwave-driven dirac currents in a topological surface band, Nature **562**, 396 (2018).